Rajesh Sadanandan, Wolfgang Meier, Johannes Heinze
Experimental study of signal trapping of OH laser induced fluorescence and chemiluminescence in flames
Appl. Phys B 106, (2012) 717-724.

The original publication is available at www.springerlink.com

http://dx.doi.org/10.1007/s00340-011-4704-z

Experimental study on signal trapping of OH laser induced fluorescence and chemiluminescence in flames

R. Sadanandan[1], W. Meier[⋆1], J. Heinze[2]

[1] Institut für Verbrennungstechnik, Deutsches Zentrum für Luft- und Raumfahrt e.V., Pfaffenwaldring 38-40, 70569 Stutttgart, Germany.
[2] Institut für Antriebstechnik, Deutsches Zentrum für Luft- und Raumfahrt e.V., Linder Höhe, D-51147 Köln-Porz, Germany.

Abstract The absorption of OH* chemiluminescence and laser-induced fluorescence (LIF) in the exhaust gas of confined premixed laminar CH_4/air flames at atmospheric pressure was investigated. One flame was used as source and a second as absorber. OH LIF was excited in the $\nu" = 0 \rightarrow \nu' = 1$ band of the A-X electronic system around $\approx$ 283 nm and spectrally resolved detected in the (0,0) and (1,1) vibrational bands around 305 - 320 nm. For OH* chemiluminescence, spectrally resolved detection was performed in the wavelength range 280 - 340 nm. For an absorption path of 54 mm and at T $\approx$ 2000 K, signal trapping on the order of 10 % - 40 % was observed. Signal trapping was most pronounced in the (0,0) band, as expected from the thermal population distribution of OH in the electronic ground state. The spectral distribution of the signals and the wavelength-dependence of the signal trapping are addressed in this paper. Implications from the results with respect to detection strategies and chemiluminescence-based equivalence ratio measurements are discussed.

1 Introduction

Laser-induced fluorescence (LIF) of OH and chemiluminescence imaging of OH radicals in the excited electronic state (OH*) have been widely used in combustion research for the determination of flame structures, temperature or heat release rate [1, 2]. Limitations in the value of these techniques can arise in flames with high OH concentrations, where absorption of laser radiation and signal trapping have often been observed [3]. With respect to laser light absorption different approaches have been proposed to mitigate the problem, e.g., using weak transitions, counter propagating laser beams, or calculation of the absorption from the detected LIF signal [4–6]. However, a remedy for signal trapping is difficult to find for different reasons. Except for well-defined laminar

flames, the spatial distribution of OH radicals including number density and energy distribution is in general unknown. Further, the internal energy distribution of the excited OH radicals after laser excitation is a dynamic process, including rotational energy transfer (RET), vibrational energy transfer (VET), and electronic quenching [7]. Although some of the involved rate coefficients are quite well known (see for example LASKIN [8]), the simulation of the time-dependent energy level redistribution after LIF excitation and the determination of the subsequent signal trapping is still a challenging task. From simple calculations or measurements it can be concluded that absorption of lines with strong line strengths is substantial even in flames of moderate size. However, the fluorescence spectrum is composed of hundreds of individual lines originating from a rapidly transforming non-thermal energy distribution. The total amount of absorption is thus not easily calculated even if the OH density along the absorption path is known. To our knowledge, a spectrally resolved study of the effect of signal trapping in OH LIF measurements in flames under well-defined boundary conditions has not been published before. It has therefore been one goal of this work, to measure the spectral distribution of OH LIF signals after passing through an absorbing gas. In most OH LIF investigations in flames, laser excitation is performed in the $\nu" = 0 \rightarrow \nu' = 1$ band of the A-X electronic system around $\approx$ 283 nm with a red-shifted detection of the fluorescence in the (0,0) and (1,1) vibrational bands around 305 - 320 nm. This scheme is also studied in this experiment using pulsed laser radiation with a pulse duration of approximately 8 ns.

Chemiluminescence imaging is usually performed using the same detection wavelength region as for LIF [9–11]. However, the rotational and vibrational distribution in the excited electronic state is generally different compared to that in LIF measurements. Nevertheless, signal trapping occurs as well and can be a serious problem in quantitative measurements of the heat release rate or equivalence ratio [12].

The second goal of the current work is therefore an experimental characterization of the signal trapping of OH* chemiluminescence under well-defined conditions and with spectrally resolved detection. Laminar premixed CH_4/air flames

---

⋆ Fax: +49-711-6862 578, E-mail: wolfgang.meier@dlr.de

were used in this study as sources for the OH emissions and confined premixed flat laminar flames were used as absorbers.The burner for the flat flames was specially designed for this purpose and consists of a square sintered bronze matrix with a close confinement of quartz plates. In this way, a quite homogeneous exhaust gas is formed with a defined boundary.

For individual emission lines the absorption depends on the population of the ro-vibrational states in the electronic ground state that can absorb the specific wavelength. For well-resolved isolated individual spectral lines, the molecular transitions for emission and absorption are mostly the same. In that case, the probability of absorption depends - besides on the line strength - on the population density of OH in the ground state which is governed by the Boltzmann distribution. For flame temperatures, e.g. at 2000 K, more than 92% of the OH radicals are in the vibrational ground state $v" = 0$. Thus, absorption for transitions from $v" = 0$ are more likely than those from higher vibrational levels. This behaviour is confirmed by the measurements reported in this paper. However, for overlapping spectral lines the situation is more complex. It must also be considered that the ro-vibrational distribution in the excited state is generally not in thermal equilibrium. The spectral distributions of the OH LIF and chemiluminescence signals is shown in this paper for a situation with negligible absorption and compared to the spectra after passing through the exhaust gas of two different laminar flames. The absorption behaviour for emission lines in the (0,0) and (1,1) vibrational bands of the A-X transition is demonstrated and quantified, and conclusions for flame investigations are derived.

2 Experimental Configuration

2.1 Burners

Photographs of the burner configuration and the flames that were used for the current investigation are shown in Fig. 1. An optically accessible, water cooled, square matrix burner, 50 x 50 mm^2 in cross section, was used as the main burner for the OH LIF measurements and a straight tube (Bunsen burner), with an inner diameter of 8 mm, was used as the main burner for the OH* chemiluminescence measurements. An identical square matrix burner was employed for the stabilization of the flames used as absorbers for both OH LIF and OH* chemiluminescence measurements (in the following termed as "absorption burner"). The sintered bronze matrix had a thickness of 18 mm and contained a copper tube for water cooling. It was custom built by the company Tridelta Siperm (material type B20, 18 μm mean pore size, 34 - 39 % porosity). The matrix resembles the ones used in the well-known McKenna burners [13]. Similar custom built matrix burners have been operated by us before with premixed CH$_4$/air and H$_2$/air flames and characterized by coherent anti-Stokes Raman spectroscopy (CARS), Rayleigh and Raman scattering. The exhaust gas temperature and composition turned out to be the same as for a McKenna burner
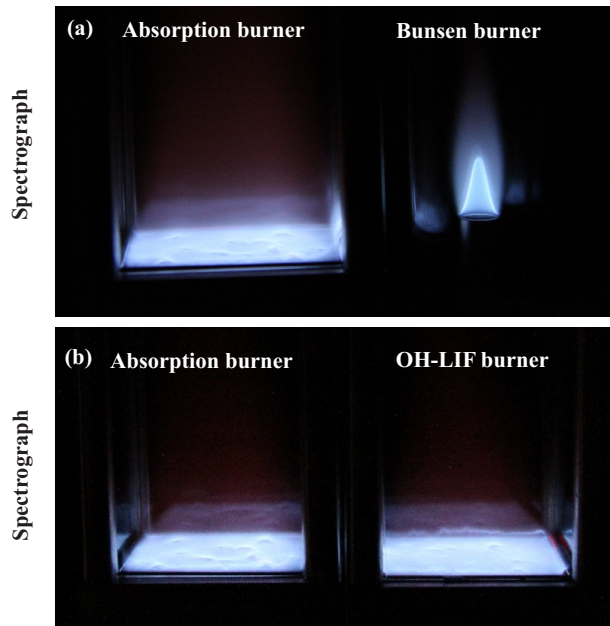

Fig. 1 Photographs showing the burner configurations that was employed in the current investigations. (a) OH* chemiluminescence signal trapping measurements (b) OH LIF signal trapping measurements

when operated with the same gas composition and flow velocity within the accuracy of the measurement techniques [14]. Thus, the exhaust gas temperatures of the flames investigated here were taken from previous measurements.

Both the main and the absorption matrix burners were equipped with quartz windows (52 x 117 mm^2, 1.7 mm thick) held by four posts at the corners. They form a confinement for the exhaust gas with an inner square section of 54 x 54 mm^2 and thus a defined absorption path. The burner for the premixed Bunsen flames consisted of a straight stainless steel tube. The flames were surrounded by a quartz tube of inner diameter 30 mm to avoid interferences from outside. The burners were operated with premixed CH$_4$/air flames stabilized under laminar conditions. The mass flow rates were regulated with high precision Coriolis (Siemens) and mass flow controllers (Brooks for the main burner and Bronkhorst for the absorption burner).

2.2 Burner operating conditions

The burners were operated at two different overall equivalence ratios, $\phi = 0.8$ and 0.9. Initial OH LIF and OH* chemiluminescence measurements were performed with the OH LIF matrix burner and the Bunsen burner operating at a constant equivalence ratio, ϕ_{LIF} and ϕ_{bunsen} respectively, and with no flame stablized at the absorption burner, $\phi_{abs} = 0$. In order to investigate the influence of OH signal trapping, the experiments were repeated by varying ϕ_{abs} while maintaining the ϕ_{LIF} or ϕ_{bunsen} constant. The flow rates for the flat flames were 26.79 slpm air and 2.25 slpm CH$_4$ for the flame with $\phi = 0.8$ and 31.99 slpm air and 3.02 slpm CH$_4$ for the

flame with $\phi = 0.9$. The flow rates for the Bunsen burner were 3 slpm air and 0.253 slpm CH_4 for the flame with $\phi = 0.8$ and 3 slpm air and 0.285 slpm CH_4 for the flame with $\phi = 0.9$.

2.3 OH LIF System

The laser system used for the OH LIF measurements consisted of a flash lamp pumped, frequency doubled Nd:YAG laser (Quanta Ray, DCR-2) pumping a frequency doubled tunable dye laser (Lumonics, HD-500) at 10 Hz. The output beam (pulse duration 8 ns and line width ≈ 0.4 cm^{-1}) from the dye laser was tuned to the $Q_1(8)$ transition of OH at approximately 283 nm in the $\nu'' = 0$, $\nu' = 1$ vibrational band of the $A^2\Sigma^+ - X^2\Pi$ system. For the initial characterization of the OH distribution of the flat flames on the matrix burner by 2D OH LIF imaging, the UV beam was expanded into a vertical light sheet by means of a combination of cylindrical and spherical lenses. The laser sheet was approximately 40 mm in height inside the flame and 400 μm in thickness at the center of the matrix. In case of the spectrally resolved OH LIF signal trapping measurements the UV beam was expanded into a horizontal sheet. A depolarizer (B.Halle Nachf., type Hanle) was placed on the beam path to avoid any influence from polarization on the LIF signal. Inside the flame the laser sheet was approximately 5 mm in width and 400 μm in thickness and had approximately 250 μJ of pulse energy. This beam geometry was chosen in order to maximize the signal passsing through the narrow entrance slit of the spectrograph and to avoid saturation (the entrance slit was parallel to the laser beam and the thickness of 400 μm was relayed onto the slit). By means of a beam splitter, a small portion of the incoming laser beam was directed into a CH_4/air reference flame on a matrix burner, operating under laminar conditions. The LIF produced by this flame was used for the online monitoring of the excitation line wavelength for both OH PLIF and spectral measurements.

2.4 Detection Systems

The schematic of the experimental set-up employed for the OH* chemiluminescence signal trapping and OH LIF signal trapping measurements are shown in Fig.2 (a) and (b) respectively.

2.4.1 Imaging system for the 2D measurements An ICCD camera (LaVision Image Intense with intensified relay optic (IRO), 1376 x 1040 pixels) equipped with a UV camera lens (Nikkor, $f/4.5$, $f = 105$ mm) and a combination of a UG11 and bandpass (295 - 340 nm) interference filter (Laser Components GmbH) was used as the detection system for the OH PLIF measurements. The captured OH PLIF images were corrected for laser sheet profile inhomogeneities in post processing using the laser sheet profile information obtained from a simultaneously captured fluorescence image of the laser sheet in a quartz cell filled with a fluorescent dye solution. OH* chemiluminescence (integrated along the line of
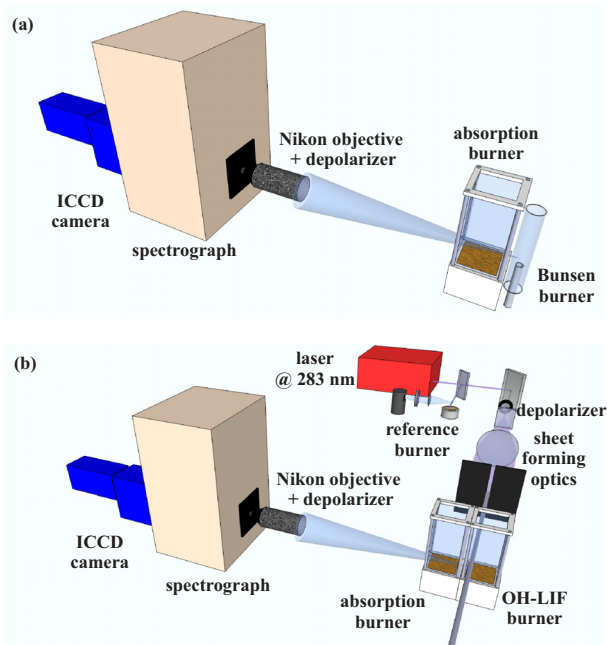

Fig. 2 Schematic of the experimental set-up used for the measurements; (a) OH* chemiluminescence signal trapping, and (b) OH LIF signal trapping

sight) was also imaged with the same detection system along with the filter combination. The exposure settings for the OH PLIF and 2D-OH* chemiluminescence measurements were 400 ns and 40 μs, respectively. All the images were also corrected for background luminosity and for the camera sensitivity. The timing between the laser pulses and the gate timings of the camera were synchronized with the help of pulse delay generator (BNC, Model 555).

2.4.2 Spectral Measurements For the OH LIF and OH* chemiluminescence spectral measurements, a spectrograph (SpectraPro 275, Acton Research Corporation, aperture ratio $f/3.8$) was used in combination with the ICCD camera (LaVision Image Intense with IRO, 1376 x 1040 pixels). The exposure settings for the OH LIF and OH* chemiluminescence measurements were 200 ns and 1 ms, respectively and the sampling rate was 10 Hz. The OH LIF signal, orthogonal to the excitation beam, and the OH* chemiluminescence signal were collected by the UV camera lens (Nikkor, $f/4.5$, $f = 105$ mm, diameter 28 mm) attached to the entrance slit of the spectrograph. A depolarizer (B. Halle Nachf., type Hanle) was placed between the UV lens and the entrance slit to mitigate any effect of polarization-dependent efficiency of the gratings. The laser sheet was at a distance of approximately 390 mm from the UV lens, leading to a detection solid angle of 4.04 x 10^{-3} sr. The spectrograph was set up with its entrance slit arranged horizontally, parallel to the laser beam, in order to capture several millimeters of the laser beam. Two different gratings, 1800 grooves/mm and 3600 grooves/mm, were used in the current measurements corresponding to dispersions of 1.75 nm/mm and 0.74 nm/mm, respectively in the spectral range of interest. The entrance slit width of the spec-

trograph was set to 150 μm. This corresponded to a spectral width of 0.26 nm (28.9 cm^{-1} at 300 nm) for the grating with 1800 grooves/mm and 0.11 nm (12.3 cm^{-1} at 300 nm) for the grating with 3600 grooves/mm. After spectral separation, the rotational bands of the OH molecule were imaged into the ICCD camera located at the exit focal plane of the spectrograph. The dependence of the detection efficiency on the wavelength was not measured, but from the data sheets of the ICCD and gratings it is expected to be small in the wavelength region of interest. 1000 laser shot measurements were performed for each operating condition. In addition, the images were binned four times on the spatial axis during measurements to achieve sufficient signal-to-noise ratio.

3 Results and Discussion

3.1 Flame characteristics

Figure 3(a) and (b) shows the time averaged OH LIF image of the matrix burner flame at $\phi_{LIF} = 0.8$ (T = 1967 K [14]) and 0.9 (T = 2110 K [14]), respectively. The flame front of both flames resides very close to the matrix within a distance of roughly 1 mm. At these temperatures and exhaust gas compositions the equilibrium OH mole fraction is 8.91 x 10^{-4} ($\phi_{LIF} = 0.8$) and 1.5 x 10^{-3} ($\phi_{LIF} = 0.9$) [15]. The laser sheet was positioned at approximately 5 mm away from the edge of the matrix burner. The laser sheet travels from left to right of the image and the variation in LIF intensity along the laser beam path is due to aborption by the OH radicals. The images shown here are an ensemble average of 200 single shots. The decrease of OH LIF signal with height above the burner is caused by a decrease of OH concentration. OH is formed in superequilibrium concentrations in the flame front and its relaxation towards chemical equilibrium takes about 3 ms [18]. The equilibrium value is reached at heights of h $\approx$ 10 - 20 mm depending on the flow velocity. The spatial position of the horizontal laser sheet for the OH LIF spectral measurements is marked in the images by the white line. The edge of the laser sheet (5 mm in width) was approximately 3 mm away from the edge of the burner matrix in direction of the detector and at a height of 17 mm. As can be seen, the laser sheet is located in a region where the OH concentration is very close to the equilibrium value. Further, the location close to the edge minimizes signal trapping within this flame.

The OH* chemiluminescence distribution from the premixed Bunsen flame is shown in Fig. 4. It has a conical shape and due to the line-of-sight integration of the chemiluminescence the edges appear more intense than the central parts. Chemiluminescence provides information about species concentation produced in the electronically excited state. The OH* chemiluminescence is formed only in the heat release zone and after a lifetime of a few nanoseconds, the excited molecules relax to lower energy levels by radiative transitions (chemiluminescence) or molecular collisions. The chemiluminescence can be absorbed by OH molecules in the absorption burner so that the detected OH* chemiluminescence intensity will only be a fraction of what was originally emitted.
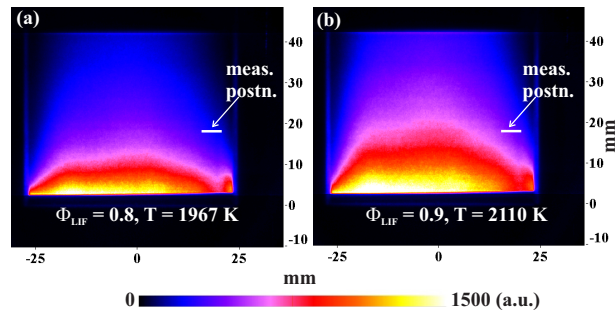

Fig. 3 2D OH LIF distribution of the investigated flames at 5 mm away from the edge of the matrix burner; also marked is the spatial poisiton in the flame where the OH LIF spectral measurements were performed

The absorption of OH* chemiluminescence signal by the OH radicals in the absorption burner is highlighted in Fig. 4(a). The top row shows the results from the Bunsen flame with $\phi_{bunsen} = 0.8$, the second row the results from $\phi_{bunsen} = 0.9$. The left images were recorded without flame on the absorption burner, the other images with absorption flames with $\phi_{abs} = 0.8$ and $\phi_{abs} = 0.9$. As expected the chemiluminescence intensity is decreased due to absorption. In Fig. 4(b) the averaged OH* chemiluminescence intensity is plotted against ϕ_{abs}. The region of the flame where the intensities were calculated is shown as a dotted rectangular region in Fig. 4(a). $\phi_{abs} = 0$ represents the case without flame in the absorption burner. The degree of signal trapping is defined here as the percent reduction in the signal intensity between the probe volume and the collection optics. It can be seen that the OH* chemiluminescence signal emitted by the Bunsen flame is dropped by approximately 17 and 16 %, for $\phi_{bunsen} = 0.8$ and 0.9, respectively, when a $\phi_{abs} = 0.9$ flame is stabilized in the absorption burner. It is noted, that the images shown do not include the chemiluminescence from the absorption flame. The absorption flame chemiluminescence was estimated by repeating the measurements without the Bunsen flame and is then subtracted from the OH* chemiluminescence distribution from the Bunsen flame in a post processing step.

In this measurement, a small contribution to the detected chemiluminescence is expected to stem from electronically excited CO_2 molecules [16]. CO_2* chemiluminescence is broadband and extends beyond the transmission range of the interference filter. A significant portion of it does not spectrally overlap with OH absorption lines and passes through the flame without being absorbed. In the imaging experiments the CO_2* contribution was not subtracted from the total chemiluminescence signal. Subtraction of it would lead to numbers larger than 17 % and 16 % for the OH* signal trapping. More details are given in the next chapter.

3.2 OH spectral distribution

The spectral distribution of the OH* chemiluminescence and OH LIF signals were analyzed with the help of the spectrograph coupled with the ICCD camera. Fig. 5(a) shows
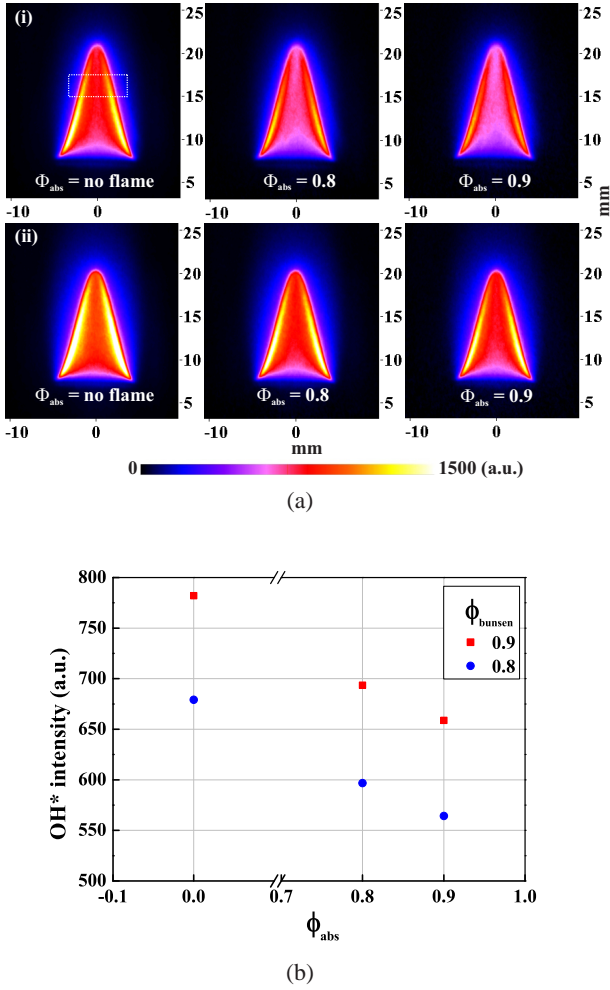
(a)

(b)

Fig. 4 (a) 2D OH* chemiluminescence distribution with changing ϕ_{abs}; (i) $\phi_{bunsen} = 0.8$, and (ii) $\phi_{bunsen} = 0.9$. (b) Corresponding OH* chemiluminescence signal intensity variation; The averaged intensities were calculated from the dashed rectangular section shown in Fig. 4(a).

the OH* chemiluminescene spectrum from the Bunsen flame stabilized at $\phi_{bunsen} = 0.9$ as seen in Fig.4(a)(ii). The imaged region was approximately 12 mm above the rim of the Bunsen burner and 17 mm above the surface of the matrix burner. The measurements were performed with the 1800 grooves/mm grating. The plot shows strong OH* chemiluminescence emissions from the A-X (0,0) band starting at a wavelength $\lambda \approx 306$ nm and also weak but non-negligible emissions from the A-X (1,0) band starting at $\lambda \approx 281$ nm. Overlaid on the (0,0) band are also weak emissions in the (1,1) band. The main portion of the chemiluminescence lies within the (0,0) band, in accordance with previous observations [9]. The signal level observed at $\lambda < 281$ nm and $\lambda > 330$ nm most probably stems from broadband CO_2* chemiluminescence [16]. While the red curve displays the distribution without absorption flame, the green one was recorded with the $\phi_{abs} = 0.9$ flame as absorber. As can be seen, significant absorption occurred in the (0,0) band and only little absorption in the (1,0) band. This is qualitatively

explained by the thermal distribution of the absorbing OH molecules which are predominantly in the vibrational ground state. Fig. 5(b) and Fig. 5(c) show the influence of absorption on the OH* chemiluminescence emissions from the (0,0) band produced by the Bunsen flame in the spectral range from 306 to 320 nm. The ϕ_{bunsen} was set to 0.8 and 0.9 in Fig. 5(b) and Fig. 5(c), respectively. The 3600 grooves/mm grating was used for these measurements. Despite the better spectral resolution of this grating, the observed lines are not isolated single transitions. For example, the line at $\lambda \approx 311.8$ nm is an overlap of at least 4 lines with the main contributions from the $P_1(8)$ and $P_2(7)$ [17]. The plots mirror the strong signal absorption that was seen earlier in the OH* chemiluminescence images. As expected, the strongest absorption is observed for the lines belonging to well-populated rotational states in the $v'' = 0$ state and those having the highest transition strengths. These are generally located in the lower wavelength region ($\lambda \approx 306$ - 313 nm). For details of the spectrum and line positions the LIFBASE spectral simulation program is recommended [17]. Increasing the temperature and the heat release rate of the Bunsen flame by increasing the equivalence ratio from 0.8 to 0.9 does not alter the observed trend significantly (see Fig. 5(c)).

From the spectra in Figures 5(b) and 5(c) the degree of signal trapping was assessed. First the contribution from CO_2* chemiluminescence was estimated from Fig. 5(a) and subtracted as a constant offset (6 a.u. in the units of Fig. 5) from the spectra. For the flame with $\phi_{bunsen} = 0.8$ (Fig. 5(b)), the absorbed intensity was 7.3 % for $\phi_{abs} = 0.8$ and 24.4 % for $\phi_{abs} = 0.9$ when the intensity was integrated over the spectral range $\lambda = 306.16$ - 320.40 nm. The relatively low signal levels in the second half of the spectra add some uncertainty to these numbers. If only the more intense spectral range $\lambda = 306.16$ - 313.0 nm is considered the numbers are 18.5 % for $\phi_{abs} = 0.8$ and 33.8 % for $\phi_{abs} = 0.9$. The corresponding signal trapping for the flame with $\phi_{bunsen} = 0.9$ (Fig. 5(c)) is 20.9 % for $\phi_{abs} = 0.8$ and 37.8 % for $\phi_{abs} = 0.9$ in the range $\lambda = 306.16$ - 320.40 nm. For the restricted range $\lambda = 306.16$ - 313.0 nm the absorbed portion is 26.1 % for $\phi_{abs} = 0.8$ and 42.6 % for $\phi_{abs} = 0.9$. These numbers are considerably larger than the ones obtained from the imaging experiments. The main reason lies in the contribution of the CO_2* chemiluminescence. Neglecting the CO_2* chemiluminescence leads to numbers that are typically a factor of 0.8 smaller. In the imaging experiments the effect is even larger because the interference filter transmits a range (295 - 340 nm) that is wider than the range $\lambda = 306.16$ - 320.40 nm considered here. It must be kept in mind that the subtraction of the CO_2* chemiluminescence background is subject to some arbitrariness because it was not determined precisely in the measurements. This is also expected to contribute to the difference in relative absorption between the flames with $\phi_{bunsen} = 0.8$ and $\phi_{bunsen} = 0.9$ when the same absorption flame was used.

For LIF an excitation strategy using the OH A-X (1-0) vibronic band is reported in literature as an option to reduce the fluorescence trapping effect [19, 20]. The corresponding fluorescence distribution and its absorption are considered in
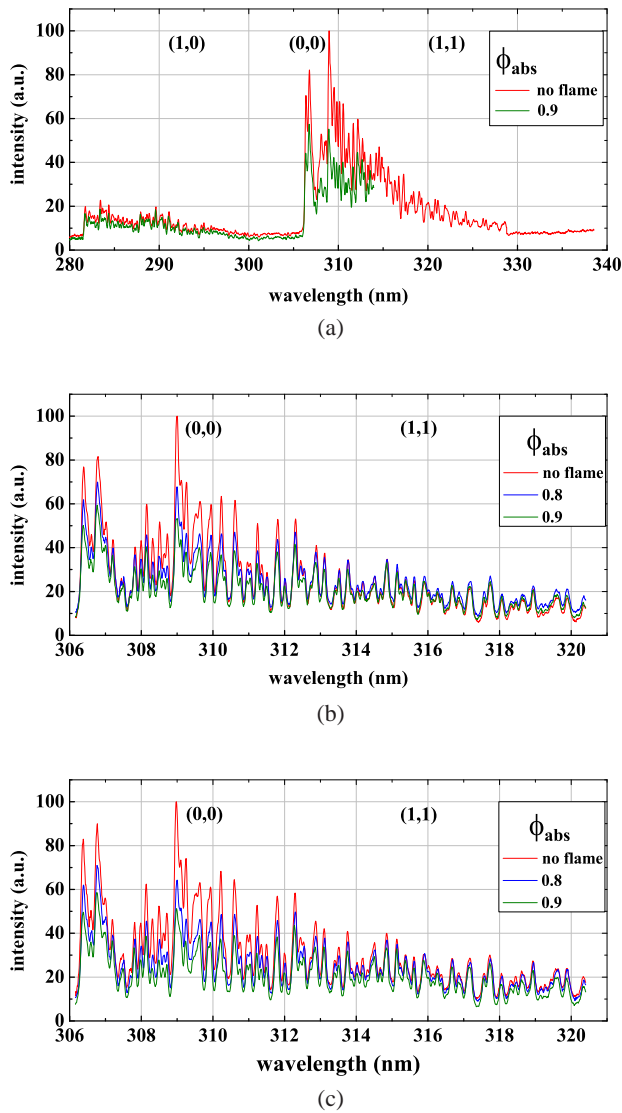
(a)

(b)

(c)

Fig. 5 OH* spectral distribution of the chemiluminescence signal from a Bunsen burner flame at $\phi_{bunsen} = 0.9$ (a), and plots showing the OH* chemiluminescence signal reabsorption from the Bunsen burner flame stabilized at $\phi_{bunsen} = 0.8$ (b) and 0.9 (c) by the absorption burner flame.

the following. Figures 6(a) and 6(b) display dispersed fluorescence spectra from the matrix flames with $\phi_{LIF} = 0.8$ and 0.9, respectively, with changes in ϕ_{abs}. The experimental configuration used for these measurements is shown in Fig. 2(b) and a 3600 grooves/mm grating was used in the spectrograph. The spectra exhibit a different shape compared to the chemiluminescence spectra because the rovibronic population distribution in the excited A-state is different. The prominent lines in the spectra are the $R_1(7)$ ($\lambda \approx 312.25$ nm), $Q_1(8)$ ($\lambda \approx 315.1$ nm), and $P_1(9)$ ($\lambda \approx 318.22$ nm) in the (1,1) band. They originate from the laser-excited rotational level N' = 8 in $\nu' = 1$. The other lines originate from rovibronic levels that have been populated by collision-induced vibrational or rotational energy transfer. Again, the red lines dis-

play the fluorescence spectra without absorbing flame and the blue and green lines correspond to the absorption flames with $\phi_{abs} = 0.8$ and 0.9, respectively. The differences between plots (a) and (b) are small. However, they are scaled to the same maximum value in the figures, but the maximum intensity is a factor of 1.96 higher for spectrum (b) due to the higher OH concentration level of the flame with $\phi_{LIF} = 0.9$. The striking feature of the spectra is the difference in absorption between the (0,0) and (1,1) band. For example, the overall OH LIF signal intensity (deduced by integrating the area under the spectrum shown) decreased by 39 % and 1.3 % in the (0,0) (calculated in the wavelength range from 306 to 312 nm) and (1,1) (calculated in the wavelength range from 312.01 to 320.4 nm) bands, respectively, for the $\phi_{LIF} = 0.8$ flame when the absorption burner is set to $\phi_{abs} = 0.9$. The corresponding values for the $\phi_{LIF} = 0.9$ flame are 43.2 % and 9.7 % for the (0,0) and (1,1) bands, respectively. Note that here the wavelength range that was selected for emissions from the (1,1) band, namely 312.01 - 320.4 nm, also includes some contribution from the (0,0) band emissions. In particular, high rotational levels of P branches (N' $\geqslant$ 8) of the (0,0) band are located in this range. So the increase in signal absorption seen in the spectral range of the (1,1) band within the $\phi_{LIF} = 0.9$ flame is also caused by the absorption of the rotational lines of the (0,0) band. The observed differences are, of course, due to the different populations in the $\nu" = 0$ and $\nu" = 1$ levels of OH in the absorption flames. Note also that the degree of absorption in the (0,0) band is on the same order as estimated for the spectrally resolved chemiluminescence measurements.

The measurements clearly convey that the absorption/trapping effects by the OH radicals in high temperature flames are non-negligible. The effects should be taken into account for quantitative measurement of OH concentrations or in diagnostic techniques in which the quatitative information is important, for example temperature measurements using OH LIF. The results also demonstrate that one way to minimize this effect is use of the (1,0) excitation strategy coupled with a detection restricted to the (1,1) emission band. As the $\nu" = 1$ vibrational level is weakly populated even at high temperatures the problem arising from radiation trapping can be mitigated. Moreover, since the (1,1) band is fluorescence shifted, the detection strategy aids in reducing laser light scattering interferences. The only practical difficulty in 2D LIF imaging is that with the commercially available bandpass filters it is not possible to spectrally discriminate the fluorescence from the (0,0) band and from the (1,1) band.

Recently, a of lot research work has been reported on equivalence ratio sensing based on the ratio of chemiluminescene intensities such as CH*/OH* [12, 21–23] or C_2*/OH* [24]. The current studies show that such quantification will be unreliable if the effect of OH* chemiluminescence signal trapping is neglected. Any such quantification is possible only if accurate corrections are made for the OH* chemiluminescence signal trapping effect, which in most of the technical combustors is difficult to achieve taking into account of the variation of OH concentration with optical depth
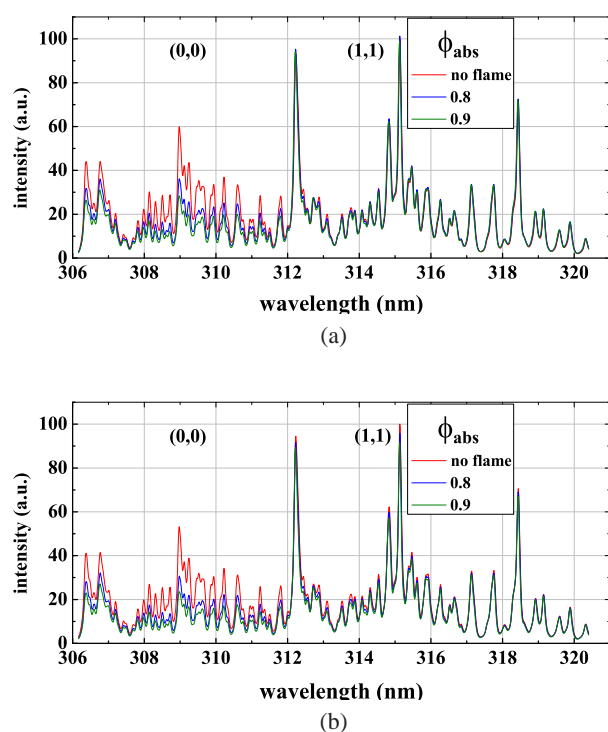
(a)

(b)

Fig. 6 Variations in OH LIF spectral distribution from the matrix burner with varying ϕ_{abs} (a) ϕ_{LIF} = 0.8, and (b) ϕ_{LIF} = 0.9.

in turbulent flames. In addition, for the validation and optimization of numerical simulations, OH LIF distribution is quite often used as a marker for the reaction zone and in some cases the OH* chemiluminescence signal as a measure of the heat release rate. But if the data used is not corrected for absorption/trapping effects, or in other way round, if these effects are not taken into account in the simulation of the OH concentration distribution that is used for comparison with the experimental results, the effectiveness of simulation codes in predicting the combustor performance under varying operating conditions will be severely restricted.

4 Summary and Conclusions

Signal trapping in OH* chemiluminescence and OH laser-induced fluorescence (LIF) measurements in flames has been investigated under well-defined experimental conditions and with spectrally resolved detection. Specially designed matrix burners with square sintered bronze flame holders have been used to stabilize flat premixed CH_4/air flames. The flames were confined by quartz plates to provide a defined boundary of exhaust gas. These flames were used as source for LIF excitation of OH and as absorption medium for LIF and chemiluminescence radiation. A premixed CH_4/air Bunsen flame was employed as source for OH* chemiluminescence. OH LIF was excited in the (1,0) band of the A-X electronic system around 283 nm and spectrally resolved detected in the (0,0) and (1,1) vibrational bands at $\lambda \approx$ 305 - 320 nm. For

OH* chemiluminescence, spectrally resolved detection was performed in the wavelength range 280 - 340 nm.

The results showed that an absorption path of 54 mm within the exhaust gas at temperatures around 2000 K led to significant absorption of both OH LIF and OH* chemiluminescence, typically on the order of 10 % - 40 %. The spectra revealed that absorption in the (0,0) vibrational band is much larger than in the (1,1) band due to the higher population density of the absorbing OH molecules in the vibrational ground state compared to that in the excited vibrational states. For the LIF measurements this fact reduces signal trapping because after excitation of $\nu' = 1$ VET is not fast enough to populate $\nu' = 0$ to an extent corresponding to thermal equilibrium. The vibrational and rotational redistribution has been well characterized in previous investigations [25, 26], however, the final effect on signal trapping has, to the authors' knowledge, not been demonstrated before with spectral resolution. OH* chemiluminescence instead is mainly concentrated in the (0,0) band and thus more prone to re-absorption.

The signal trapping of OH* chemiluminescence should carefully be considered in measurements of heat release rates [10, 11] or equivalence ratio based on the ratio of OH*/CH* [11, 12]. It is most likely that CH* chemiluminescence is hardly absorbed by the flame due to the low overall CH concentration, so that the OH*/CH* ratio changes due to the OH* chemiluminescence trapping. In any applications where OH LIF measurements are quantitatively evaluated signal trapping may also lead to errors, in particular, in large combustion chambers at high temperature and pressure. For planar LIF applications an optical long pass filter with a very sharp edge at $\lambda \approx$ 312 nm would help in the way that it only transmits the fluorescence in the (1,1) band. However, such a filter is hardly available and would lead to a significant signal reduction.

References

1. A.C. Eckbreth, *Laser Diagnostic for Combustion Temperature and Species* (Gordon and Breach, Netherlands 1996).
2. K. Kohse-Höinghaus, J. Jeffries (Eds.), *Applied Combustion Diagnostics* (Taylor & Francis, New York 2002).
3. J.W. Daily, Prog. Energy Combust. Sci., **23** (1997) 133-199.
4. D. Stepowski, Proc. Combust. Inst., **23** (1990) 1839-1846.
5. M. Versluis, N. Georgiev, L. Martinsson, M. Aldén, S. Kröll, Appl. Phys. B, **65** (1997) 411-417.
6. R. Giezendanner-Thoben, U. Meier, W. Meier, J. Heinze, M. Aigner, Appl. Opt., **44** (2005) 6565-6577.
7. K. Kohse-Höinghaus, Prog. Energy Combust. Sci., **20** (1994) 203-279.
8. A. Bütler, U. Lenhard, U. Rahmann, K. Kohse-Höinghaus, and A. Brockhinke, Proc. of LACEA, **TuE4** (2004).
9. J.G. Lee, D.A. Santavicca, J. Propulsion and Power, **19** (2003) 735-750.
10. L.C. Haber, U. Vandsburger, Combust. Sci. Technol., **175** (2003) 1859-1891.
11. C.S. Panoutsos, Y. Hardalupas, A.M.K.P. Taylor, Combust. Flame, **156** (2009) 273-291.
12. V.N. Nori, Ph.D thesis, Georgia Institute of Technology (2008).

13. http://www.flatflame.com/

14. P. Weigand, R. Lückerath, W. Meier, *Documentation of Flat Premixed Laminar CH₄/Air Standard Flames* (http://www.dlr.de/vt)

15. C. Morley, *A Chemical Equilibrium Program for Windows* (http://www.c.morley.dsl.pipex.com/)

16. J.M. Samaniego, F.N. Egolfopoulos, C.T. Bowman, Combust. Sci. Technol., **109** (1995) 183-203.

17. J. Luque, D.R. Crosley, SRI International Report MP99-009 (1999)

18. R. Sadanandan, M. Stöhr, W. Meier, Appl. Phys. B, **90** (2008) 609-618.

19. P. Desgroux, L. Gasnot, J.F. Pauwels, L.R. Sochet, Appl. Phys. B, **61** (1995) 401-407.

20. N.M. Laurendeau, J.E.M. Goldsmith, Combust. Sci. Technol., **63** (1989) 139-152.

21. T.S. Cheng, C.-Y. Wu, Y.-H. Li, Y.-C. Chao, Combust. Sci. Technol., **178** (2006) 1821-1841.

22. N. Docquier, F. Lacas, S. Candel, Proc. Combust. Inst., **29** (2002) 139-145.

23. T.M. Muruganandam, B.-H. Kim, M.R. Morrell, V. Nori, M. Patel, B.W. Roming, J.M. Seitzman, Proc. Combust. Inst., **30** (2005) 1601-1609.

24. J. Kojima, Y. Ikeda, T. Nakajima, Combust. Flame, **140** (2005) 34-45.

25. A.T. Hartlieb, D. Markus, W. Kreutner, K. Kohse-Höinghaus, Appl. Phys. B, **65** (1997) 81-91.

26. R. Kienle, A Jörg, K. Kohse-Höinghaus, Appl. Phys. B, **56** (1993) 249-258.